Structural and electronic properties of luminescent copper(I) halide complexes of bis[2-(diphenylphosphano)phenyl] ether (DPEphos). Crystal structure of [CuCl(DPEphos)(dmpymtH]†

P. Aslanidis,*[a] P. J. Cox[b] and A. C. Tsipis*[c]

Received 10th April 2010, Accepted 30th July 2010
DOI: 10.1039/c0dt00286k

Heteroleptic copper(I) halide complexes containing the bis[2-(diphenylphosphano)phenyl]ether (DPEphos) ligand and the heterocyclic thioamides pyridine-2(1H)-thione (py2SH), pyrimidine-2(1H)-thione (pymtH) or 4,6-dimethylpyrimidine-2(1H)-thione (dmpymtH) have been synthesized and characterized by ^{1}H-NMR, IR spectroscopy, elemental analyses and melting point determinations. The complexes can be readily obtained by the addition of the thione ligand to a CuX–diphosphane adduct in dichloromethane–ethanol solution. The molecular structure of [CuCl(DPEphos)(dmpymtH)] complex has been established by single-crystal X-ray diffraction. The structure features a tetrahedral copper(I) center with two phosphorus atoms from the chelating diphos ligand, one halogen atom and the exocyclic sulfur atom of the heterocyclic thioamide unit. The complexes are strongly emissive in the solid state at ambient temperature. DFT and TD-DFT calculations were employed to study the structural, electronic and photophysical properties of the novel complexes. Electronic absorption spectra show two broad bands in the regions 275–290 and 380–398 nm of mixed MLCT/IL character. Intense blue–green emission is observed in the region 500–558 nm for complexes having py2SH or dmpymtH thione ligands. The emitting first triplet excited state, T_1 is mainly localized on the thione ligand.

1. Introduction

In the past two decades, coordination compounds of many transition metals have attracted considerable interest, stimulated by their real or potential applications as components for luminescent-based chemical sensors,[1–4] in display devices,[5,6] as dopants to increase the electroluminescence efficiency of organic light emitting diodes (OLEDs and PHOLEDs),[7–9] as sensitizers in solar-energy conversion,[10,11] as photocatalysts and photoinitiators. First row transition metal compounds are attractive from an economical viewpoint, while they are less toxic and more easily available than the currently used third row noble metal complexes which are expensive, toxic and difficult to obtain. In particular, copper(I) complexes are beginning to receive particular attention,[12,13] with the most intensively studied and very promising class involving polypyridine and phenanthroline luminophores,[14,15] newly combined with bis[2-(diphenylphosphano)phenyl]ether (DPEphos) as a second rigid chelating ligand.[16–20] McMillin *et al.*[21–23] reported that the copper(I) complex $[Cu(dmphen)_2]^+$, where dmphen = bis(2,9-dimethyl-1,10-phenanthroline) although exhibits photoluminescence in CH_2Cl_2 it is not emissive in methanol, ethanol or acetonitrile solutions. In contrast, $[Cu(I)(1,10\text{-phenanthroline})_2]^+$ is non-emissive indicating the key role of the substituents at 2,9-positions of phenanthroline ligand which prevent large structural distortions of the excited states.[21–23] The impact on luminescence properties upon modifying the molecular structure was demonstrated in the case of $[Cu(dmphen)_2]X$ ($X = BF_4^-$, ClO_4^-, NO_3^- and Cl^-) complexes.[24] In the latter, changing the counteranion, X^-, results in a decrease of the dihedral angle between the two dmphen ligands and to a concomitant reduction in the emission lifetimes. Mixed-ligand copper(I) complexes have been synthesized and tested for their ability to overcome solvent-induced exciplex quenching of phosphorescence lifetime. Among them the most promising are copper(I) complexes with polypyridine and phenathroline ligands of the general formula $[Cu(NN)(POP)]^+$ (NN = phenanthroline, POP = bis[2-(diphenylphosphano)phenyl]ether).[25]

Despite the relatively large amount of experimental work devoted to the luminescence properties of copper(I) complexes, theoretical studies are rather scarce. An extensive experimental work accompanied by a detailed theoretical analysis of the photophysical properties of copper(I) bis(diimine) compounds was reported by Nozaki *et al.*[26] In a combined experimental–theoretical study it was shown that for a series of mixed-ligand copper(I) complexes, $[Cu(NN)(POP)]^+$, the HOMO–LUMO gap

[a]*Aristotle University of Thessaloniki, Faculty of Chemistry, Inorganic Chemistry Laboratory, P.O. Box 135, GR- 541 24, Thessaloniki, Greece. E-mail: aslanidi@chem.auth.gr*
[b]*School of Pharmacy, The Robert Gordon University, Schoolhill, Aberdeen, AB10 1FR, Scotland. E-mail: p.j.cox@rgu.ac.uk*
[c]*Laboratory of Inorganic and General Chemistry, Department of Chemistry, University of Ioannina, 451 10, Ioannina, Greece. E-mail: attsipis@uoi.gr*

† Electronic supplementary information (ESI) available: The structural parameters of complexes **1–9** in their S_0 and T_1 states and their differences are given in Tables S1 and S2 respectively. The principal singlet–singlet optical transitions for the absorptions of **1–6**, **8** and **9** are compiled in Tables S3–S11. The absorption and emission spectra of complexes **1–9** computed with TD-DFT calculations at the PEB0/Def2-TZVP levels in the gas phase and in CH_2Cl_2 solution are given in Fig. S1 and S2. The cartesian coordinates and energy data of the stationary points on the potential energy surface of the [CuCl(DPEphos)(thione)] complexes (**1–9**) in both the S_0 and T_1 states (Table S11). The IR and normal modes of complexes **1–6**, **8** and **9** in the S_0 and T_1 states are shown in Fig. S3–S8. CCDC reference number 768855. For ESI and crystallographic data in CIF or other electronic format see DOI: 10.1039/c0dt00286k

plays a crucial role in modulating the photophysical properties of the complexes.[25]

Our interest in exploring the photochemistry of mixed-ligand copper(I) complexes incorporating chelating phosphanes in the coordination sphere has evolved from our recent studies on a series of Cu(I) compounds formulated as [Cu(κ³-triphos)(thiolate)].[27] Noticeably, the presence of thiolate, acetylide and/or phosphane ligands favors formation of ligand-linked metal cluster arrays through metal–metal interactions.[28] The emission energy, lifetime and quantum efficiency of Cu(I) thiolate complexes are tunable by modifying the ligands as well as introducing electron-donating or -accepting substituents to the aromatic rings. In this work, we employed computational (DFT and TD-DFT) methodologies in conjunction with single crystal X-ray data aiming to contribute to the understanding of the relationship between structure and photophysical properties, and in this particular case to evaluate the impact of the thiolate ligand on the luminescence properties of the compounds. Accordingly we wish to report on new luminescent derivatives resulting from the reactions of copper(I) halides with bis[2-(diphenylphosphino)phenyl]ether (DPEphos) and some neutral heterocyclic thiones.

2. Results and discussion

2.1. General considerations – synthesis and spectroscopic characterization

Reaction of copper(I) halides with DPEphos and a heterocyclic thioamide ligand in dry dichloromethane–ethanol mixtures gives good yields of the complexes [CuX(DPEphos)(thione)] (X = Cl, Br, I and thione = pyridine-thione, pyrimidine-2-thione and 4,6-dimethylpyrimidine-2-thione). The diphosphane and heterocyclic thione ligands along with their abbreviations are given in Scheme 1.

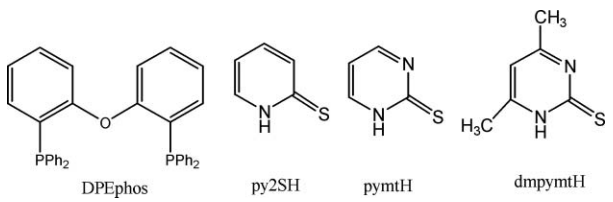

Scheme 1 The diphosphane and heterocyclic thiones used as ligands with their abbreviations.

The yellow to orange coloured microcrystalline solids are diamagnetic and soluble in dichloromethane, chloroform and acetone. Their dichloromethane solutions are non-conducting.

The electronic absorption spectra of complexes **1–9**, recorded in dichloromethane at room temperature, show two intense broad bands with maxima in the 275–290 and 380–398 nm regions respectively. With reference to the absorption of the uncoordinated DPEphos (272 nm), the first one can be attributed to intraligand $\pi \rightarrow \pi^*$ transitions on the phenyl groups of the phosphane ligand, whereby the lower energy band, which lies in the region where the free thiones absorb, expressing a small red shift as a consequence of the coordination to Cu(I), should be considered as a thione-originating intraligand transition.

The infrared spectra of compounds **1–9** recorded in the range 4000–250 cm^{-1} contain, apart from the strong vibrational phosphane bands, which remain practically unshifted upon co-ordination, the characteristic four "thioamide bands" due to the presence of the heterocyclic thione ligands, with shifts indicative of an exclusive S-coordination mode, as well as a broad band in the 3430–3460 cm^{-1} region assigned to the ν(NH) stretching vibration.

Compounds **1–3** and **7–9** exhibit an intense blue–green emission with λ_{max} values of the broad bands in 500–558 nm range when excited at λ = 350 nm at room temperature in the solid state, while the emissions observed for compounds **4–6**, containing the pyrimidine-2-thione ligand, are extremely weak. The absorption and emission spectra of a representative compound **2** are shown in Fig. 1 while absorption and emission data of the complexes under investigation are summarized in Table 1.

Table 1 Absorption and emission maxima of [CuX(DPEphos)(thione)] complexes at room temperature

Complex	λ_{max}/nm[a]	λ_{em}/nm[b]
[CuCl(DPEphos)(py2SH)], **1**	275, 390	513
[CuBr(DPEphos)(py2SH)], **2**	289, 387	534
[CuI(DPEphos)(py2SH)], **3**	285, 386	500
[CuCl(DPEphos)(dmpymtH)], **7**	278, 393	549
[CuBr(DPEphos)(dmpymtH)], **8**	284, 388	558
[CuI(DPEphos)(dmpymtH)], **9**	290, 380	527

[a] Solution in CH_2Cl_2. [b] Solid state.

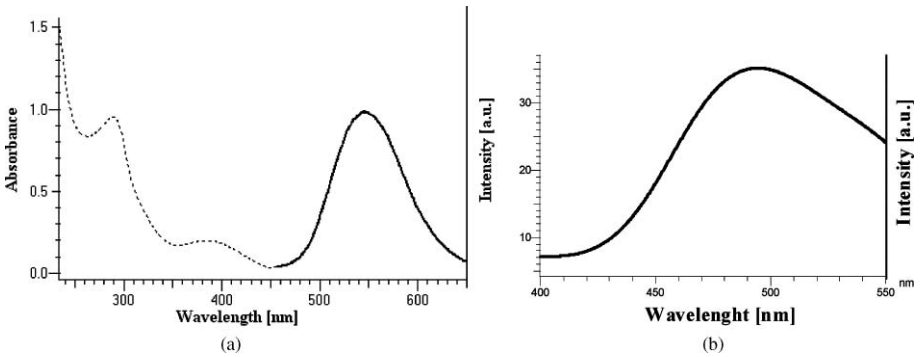

Fig. 1 (a) Room temperature electronic absorption (in CH_2Cl_2 solution, dashed line, left axis) and emission (solid state, λ_{exc} = 350 nm, solid line, right axis) spectra and (b) emission spectrum in CH_2Cl_2 solution of [CuBr(DPEphos)(py2SH)], **2** complex.

2.2 X-Ray structure†

The single crystal structure of [CuCl(DPEphos)(dmpymtH)] (complex **7**) was resolved. An ORTEP view is depicted in Fig. 2, and the coordination and geometrical parameters are listed in Table 2. The molecule adopts a slightly distorted tetrahedral geometry around the copper center with a P–Cu–P angle of 107.57(3)°, which is clearly smaller than the values of 111.51(5)° and 116.44 (4)° observed for $[Cu(NCNMe_2)_2(DPEphos)]BF_4$[29] and [Cu(dmp)(DPEphos)]BF_4[30] complexes respectively.

The two P–Cu bond distances are 2.2966(7) and 2.2829(8) Å respectively, and thus somewhat longer than those found in [Cu(DPEphos)(acac)],[31] or in $[Cu(DPEphos)_2]BF_4$[32] complexes. The two phenyl rings in the backbone of the DPEphos ligand form an angle of 80.01(9)°, which is much larger than the corresponding angle of the free diphosphane [*ca.* 67°], but comparable to the values generally found in other related compounds.[27] Furthermore, the distance of 3.6948(1) Å between the two P atoms is significantly shorter than that found in the free DPEphos [5.741(1) Å]. The Cu–S and Cu–Cl bond distances of 2.3186(8) and 2.3629(7) Å respectively are within the range of values previously found in complexes with a similar $CuClSP_2$ structural core.[33–36]

It is worth noting that the ether O atom is located at a non-bonding distance of 3.3400(19) Å from the metal center. As in many other copper(I) halide complexes containing heterocyclic thione ligands, a strong intramolecular hydrogen bridge [N(2)–H(2) = 0.880 Å, NH(1)–Cl(1) = 2.160 Å, Cl(1)···N(2) = 3.038 Å, Cl(1)···H(2)–N(2) = 176°] contributes to further stabilization of the molecule in the solid state.

Table 2 Selected bond lengths [Å] and angles [°] for **7**

Cu(1)–Cl(1)	2.3629(7)	Cu(1)–S(1)	2.3186(8)
Cu(1)–P(1)	2.2966(7)	S(1)–C(1)	1.703(3)
Cu(1)–P(2)	2.2829(8)		
P(1)–Cu(1)–P(2)	107.57(3)	P(2)–Cu(1)–Cl(1)	114.24(3)
P(1)–Cu(1)–S(1)	109.96(3)	S(1)–Cu(1)–Cl(1)	109.03(3)
P(2)–Cu(1)–S(1)	114.34(3)	C(1)–S(1)–Cu(1)	114.09(11)
P(1)–Cu(1)–Cl(1)	100.80(3)	C(20)–O(1)–C(30)	116.3 (2)

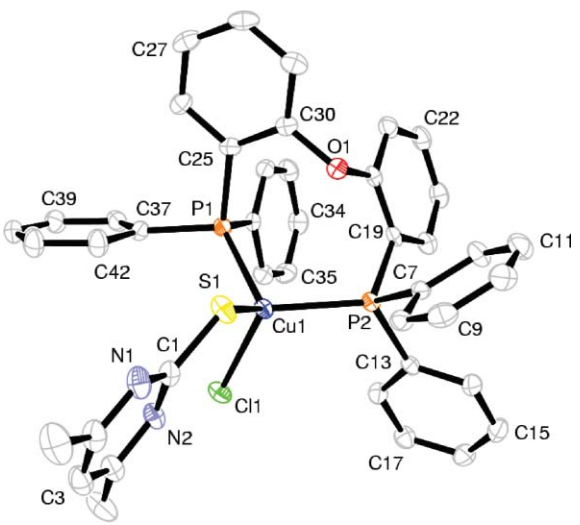

Fig. 2 A view of [CuCl(DPEphos)(dmpymtH)] (**7**) with atom labels. Displacement ellipsoids are shown in the 50% probability level.

2.3 Computational studies

2.3.1 Electronic structures at the optimized S_0 and T_1 geometries. The study of the phosphorescent properties of transition metal compounds requires knowledge of the degree of structural distortion on going from the singlet S_0 ground state to the emitting triplet T_1 state. This factor along with the energy difference between these two states, $E(T_1) - E(S_0)$ are of significant importance since they are related to the non-radiative decay rate of a complex. For an effective phosphorescent transition metal compound the structural distortion accompanying the S_0 to T_1 transition should be small. In contrast, the T_1–S_0 energy gap should be large in order for the non-radiative decay to be minimized or preferably eliminated according to the energy gap law which states that the non-radiative decay of a transition metal complex increases exponentially as the energy gap or emission energy decreases.[37] Therefore, we have employed density functional theory calculations to optimize the geometry of complexes **1–9** in their S_0 singlet ground state as well as in their T_1 triplet state. The structural parameters of complexes **1–9** along with the changes of selected structural parameters accompanying the S_0 to T_1 excitation calculated at the PBEO/Def2-TZVP level are compiled in Tables S1 and S2 given in ESI.†

The optimized structural parameters of **7** in the S_0 ground state are in good agreement with the X-ray structural analysis data. However, the PBE0/Def2-TZVP computational protocol overestimates the coordination bond lengths by 0.04–0.06 Å, while the respective bond angles defining the coordination sphere of the complex showed a deviation in the range 0.4 to 5.4°. It should be noted that the most significant structural changes accompanying the S_0 to T_1 transitions of complexes **1–9** are focused on the coordination sphere of the complexes, *i.e.* the M–L bond lengths and L′–M–L bond angles, while the rest of the structural parameters remain practically unaffected. The structural changes on the phenyl rings of the phosphane and thione ligands present very small or even no changes upon going from the S_0 to the T_1 state. Therefore, we will focus our attention only on the changes in the bond lengths and angles in and near the copper coordination sphere occurring during the S_0–T_1 transition. An inspection of Tables S1 and S2 reveals that in all complexes there is a shortening of the Cu–X (X = Cl, Br or I), Cu–S and Cu–P2 bond lengths by 0.08–0.15 Å, 0.11–0.14 Å and 0.02–0.03 Å respectively along the S_0 to T_1 route.

In contrast, there is an elongation of Cu–P1 bond in the T_1 state by 0.09–0.13 Å as compared to that found for the S_0 ground state of complexes **1–9**. The same holds true for the S–C1 and C1–N bonds of the thione ligand which are lengthened by 0.05–0.08 Å and 0.004–0.030 Å in the T_1 state. Finally, as we move further away from the copper coordination sphere the changes in bond lengths between the S_0 and T_1 states become negligible or even zero (see Tables S1 and S2, ESI†).

The bond angles mostly affected during the S_0–T_1 transition are the <(X–Cu–S) and <(S–Cu–P1). The former becomes more obtuse while the latter becomes more acute with the changes falling in the ranges 9–16° and 0–7° respectively. For the rest of the bond angles around or near the copper metal center namely the <(P1–Cu–P2), <(P2–Cu–X), <(Cu–P1–C10) and <(Cu–P2–C12), only minor changes are observed falling in the range −3–5°. In addition, in going from the S_0 to the T_1 state, significant changes occur in

Table 3 Energetic parameters relevant to phosphorescence of complexes **1–9** and differences in Mulliken charges between the S_0 and T_1 states calculated at the PEB0/Def2-TZVP level of theory

Parameter	**1**	**2**	**3**	**4**	**5**	**6**	**7**	**8**	**9**
$\Delta E_{T_1-S_0}$/kcal mol^{-1}	52.9	52.6	51.9	47.2	46.9	46.4	53.6	51.6	51.1
Δdd_{occ}/eV	0.26	0.24	0.19	0.26	0.23	0.20	0.20	0.21	0.19
ΔE_{0-0}/eV	2.21	2.20	2.17	1.98	1.96	1.95	2.28	2.17	2.14
ΔE_{ver}/eV	1.81	1.73	1.69	1.20	1.22	1.26	1.66	1.48	1.48
λ_{vib}/eV	0.48	0.55	0.56	0.85	0.82	0.75	0.67	0.76	0.73
ΔQ_{Pt}	0.03	0.03	0.04	0.01	0.03	0.04	0.07	0.03	0.05
ΔQ_S	–0.12	–0.12	–0.11	–0.07	–0.07	–0.06	–0.03	–0.08	–0.08
ΔQ_X	–0.05	–0.07	–0.09	–0.07	–0.09	–0.11	–0.03	–0.09	–0.12
ΔQ_{P1}	–0.06	–0.06	–0.06	–0.06	–0.06	–0.06	0.08	–0.06	–0.05
ΔQ_{P2}	0.00	0.00	0.00	0.00	0.00	0.00	0.00	0.00	0.00

the conformation of the thione and phenyl rings which are twisted by 5–31° and 7–76° respectively. On the other hand, the dihedral angle P1–C12–C13–O changes to a lesser extent by 7–10°.

The energy difference $\Delta E_{T_1-S_0} = E(T_1) - E(S_0)$ between the singlet ground state, S_0 and the triplet first excited state, T_1, calculated at the PEB0/Def2-TZVP level of theory is compiled in Table 3. The $\Delta E_{T_1-S_0}$ is taken as the total electronic energy difference between the T_1 and S_0 states (Scheme 2).

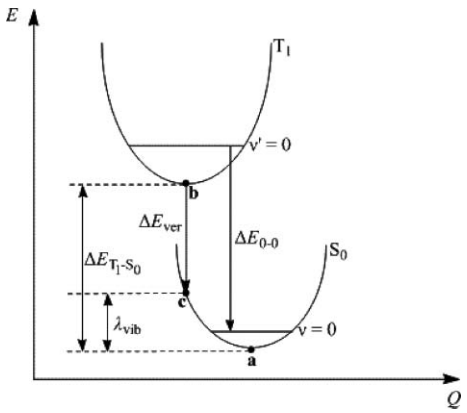

Scheme 2 Potential energy curves of S_0 and T_1 states and energetic parameters relevant to phosphorescence.

The decrease of the $\Delta E_{T_1-S_0}$ energetic parameter follows the order **1** > **2** > **3** > **8** > **9** > **4** > **5** > **6** > **7** and based on the energy gap law, the non-radiative rate constant, k_{nr} of these complexes is expected to increase in the same order. In general, the $\Delta E_{T_1-S_0}$ energy gap depends on the nature of the thione ligand following the trend py2SH > dmpymtH > pymtH. The exception is complex **7**, which although bears the dmpymtH ligand, exhibits the lowest $\Delta E_{T_1-S_0}$ energy gap and subsequently is expected to have the largest non-radiative decay rate constant, k_{nr}. On the other hand, amongst the copper(I) complexes with py2SH or pymtH thione ligands, the $\Delta E_{T_1-S_0}$ energy gap depends on the nature of the halide ligands following the trend Cl^- > Br^- > I^-. However, this is not true for the copper(I) complexes with dmpymtH thione ligand where the $\Delta E_{T_1-S_0}$ energy gap follows the trend Br^- > I^- > Cl^-. Another factor which has been stated as being critical in determining the phosphorescence efficiency of a transition metal complex[38,39] is the energy splitting, Δdd_{occ} of its highest occupied d orbitals.

Accordingly, if the closer in energy the highest d occupied orbitals are, the larger the H_{soc} matrix element between the S_1 and T_1 states will be, resulting in higher radiative decay rate constant, k_r (faster radiative decay). Therefore, we have calculated the energy splitting, Δdd_{occ} of the highest occupied d orbitals (actually they are MOs having mainly d orbital character) of complexes **1–9** and the results are given in Table 3.

Perusal of Table 3 reveals that Δdd_{occ} is highest when the halide ligand is chloride and lowest when it is iodide. Also, amongst the complexes with the same halide ligand, the lowest Δdd_{occ} is observed for those having dmpymtH as the thione ligand (with the exception of complexes **3** and **9**).

In Table 3 are also given the 0–0 transition energies, ΔE_{0-0}, (Scheme 2) for complexes **1–9** to help rationalize the electronic origin of peaks in the emission spectra. The 0–0 transition energy ΔE_{0-0} is computed from the difference in total energies of the optimized S_0 and T_1 states taking into account the respective zero-point energies (ZPE) of complexes **1–9**.

In addition, two other energetic parameters of interest have been calculated, namely the vertical transition energy, ΔE_{ver} and the vibrational reorganization energy, λ_{vib}. The former is obtained by total electronic energy difference between the T_1 and the S_0 state at the T_1 optimized geometry and the latter is taken as the total electronic energy difference between the S_0 and the S_0 state at the T_1 optimized geometry (Scheme 2). The calculated values are also given in Table 3. The vertical transition energy, ΔE_{ver} for complexes **1–3** and **7–8** correspond to transitions in the visible region while for complexes **4–6** in the near IR region. Complexes **4–6** show the largest vibrational reorganization energy, λ_{vib} while the lowest ones are observed for complexes **1–3**.

An alternative way to describe the emitting lowest triplet state, T_1 is through Mulliken population analysis allowing the estimation of the changes of the net atomic charges upon the $T_1 \rightarrow S_0$ de-excitation process. Perusal of Table 3 reveals that upon the $T_1 \rightarrow S_0$ de-excitation, charge is transferred from the copper central metal atom (positive ΔQ_{Cu}) to the surrounding donor atoms (negative ΔQ_S, ΔQ_X and ΔQ_{P1}) with the exception of P2 donor atom ($\Delta Q_{P2} = 0$). However, this does not hold true for complex **7** where in the $T_1 \rightarrow S_0$ de-excitation process the atom losing electron density is P1 while the atoms gaining electron density are Cu, S and Cl. It should be noted that the changes in net atomic charges during the $T_1 \rightarrow S_0$ de-excitation process are relatively small.

The spin density of a representative complex **1** in its lowest triplet excited state, T_1 obtained as the difference between α and β spin contributions to the total electron density, is depicted in Fig. 3 along with the 3D contour plots of the singly occupied

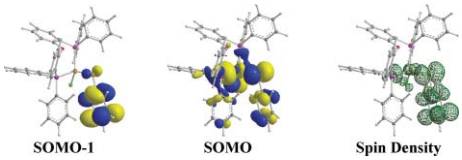

Fig. 3 3D contour plots of SOMO and SOMO-1 along with spin density isosurface (0.001 au) of complex **1** computed at the PEB0/Def2-TZVP level.

molecular orbitals (SOMOs). Analogous are the spin densities and the SOMOs of the remaining complexes.

Inspection of Fig. 3 reveals that the spin density is mainly distributed on the thione and halide ligands and to a lesser extent on the Cu metal center as well as on one P donor atom. The spin density distribution is approximately accounted for by the sum of the SOMO and SOMO-1. Thus, upon decay from the T_1 to S_0 state, polarization of the spin will involve mainly recoupling of the electron in the SOMO with the electron residing in the SOMO-1 since in the singlet state spin density is identically zero at every point in space. Taking into account the shapes of the molecular orbitals and the spin density in the T_1 state, it seems that the electron is localized mainly on thione ligand while the hole is localized on the metal.

2.3.2 TD-DFT simulated absorption spectra. The absorption spectra of complexes **1–9**, were computed with TD-DFT calculations at the PEB0/Def2-TZVP level on the optimized singlet ground states of the complexes in the gas phase and in CH_2Cl_2 solution. The simulated absorption spectra of a representative complex **2** in the gas phase and in CH_2Cl_2 solution are depicted schematically in Fig. 4, while those of the remaining complexes are given in ESI (Fig. S1 and S2).†

Selected TD-DFT principal singlet–singlet electronic transitions, excitation energies and oscillator strengths for the gas phase and CH_2Cl_2 solution spectra of the representative complex **2** are compiled in Table 4. The singlet–singlet electronic transitions, excitation energies and oscillator strengths of complexes **1–9** are given in more detail in the ESI (Tables S3–S11).†

It should be noted that the absorption spectra are marginally affected by changing either the halide or the thione ligand, basically exhibiting the same qualitative features *i.e.* an intense high energy band with a shoulder in the ultraviolet region (250–350 nm) and a lower energy band of very low intensity in the visible region (400–450 nm). Noteworthy the simulated absorption spectra of complexes **1–9** in CH_2Cl_2 solution are in close resemblance with the experimentally obtained absorption spectra. An inspection of Table 4 reveals that the electronic transitions are blue shifted and gain intensity in the CH_2Cl_2 solution spectra of the complexes compared to the simulated spectra in the gas phase.

The low-energy absorption band of very low intensity involves in all cases, mainly a HOMO → LUMO excitation and in some cases (**2**, **3** and **9**) involves also a HOMO-1 → LUMO excitation (Table 4). In Fig. 5 are depicted schematically the 3D contour surfaces plots of the molecular orbitals involved in the electronic transitions for a representative complex **7** while analogous are the MOs involved in the electronic transitions of the remaining complexes.

Inspection of Fig. 5 reveals that the HOMO and HOMO-1 are constructed from the out-phase combination of Cu 3d AOs with p orbitals located on the S atom of the thione ligand and on the halide ligand as well, while LUMO is mainly located on the thione ligand. Therefore, the low-energy absorption band exhibits a composite electronic transition pattern involving both MLCT and intraligand, IL transitions. The electronic transitions are allowed under the electric dipole interaction since the corresponding computed transition dipole moments, μ are non-zero while the % *CT* values are positive, indicating MLCT character. The charge transfer, taking place upon the electronic transitions responsible for the low-energy bands, is reflected on the changes of the electron density distribution depicted in Fig. 6 in the form of electron density difference maps (EDDM) for the representative complex **7**. Accordingly, the region comprising the metal and the surrounding atoms, including the S atom of the thione and the halide ligand, is depleted from electron density in contrast to the region comprising the thione ligand where there is an enhancement of the electron density.

The simulated absorption spectra of all complexes **1–9** exhibit also a broad, very intense high-energy band arising from a multitude of electronic transitions. The most important electronic transitions relevant with the high-energy band, involve HOMO, (HOMO-1 to -3) → LUMO, (LUMO+1 to +9) excitations. As it has already been mentioned, HOMO and HOMO-1 are located

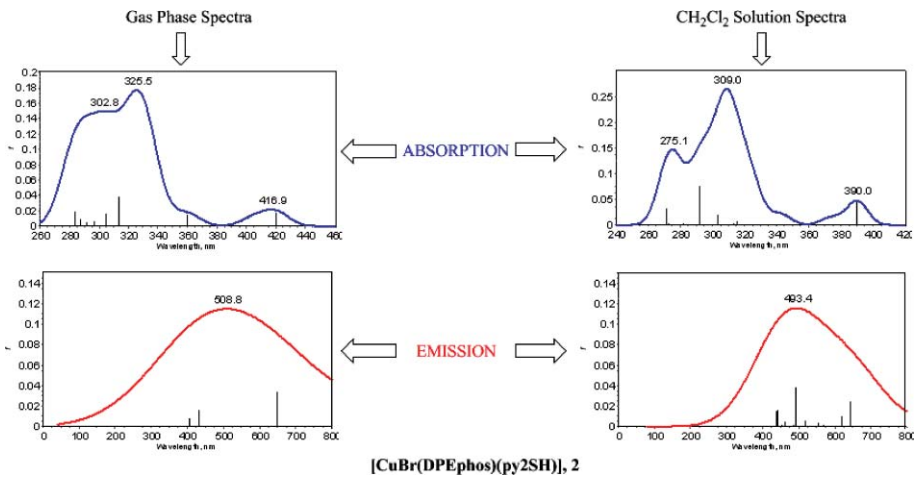

Fig. 4 TD-DFT-PBE0/Def2-TZVP simulated absorption and emission spectra of a representative complex **2** in the gas phase and in CH_2Cl_2 solution.

Table 4 Selected principal singlet–singlet optical transitions in the absorption spectra of complex **2** in the gas phase and CH_2Cl_2 solution calculated at the TD-DFT-PBEO/Def2-TZVP level

Excitation (% composition)	E/eV	λ/nm	OS, f	μ	% CT
Gas phase					
H-1 → L (19%), H → L (75%)	2.951	420.2	0.018	0.504	16
H → L+1 (94%)	3.445	359.9	0.016	0.428	16
H → L+2 (39%), H → L+3 (40%)	3.692	335.9	0.035	0.621	13
H → L+3 (10%), H → L+4 (10%)	3.767	329.2	0.048	0.721	3
H → L+3 (15%), H → L+4 (61%)	3.783	327.8	0.053	0.759	15
H → L+4 (17%), H → L+5 (60%)	3.885	319.2	0.029	0.553	13
H-1 → L+2 (29%), H-1 → L+3 (53%)	3.954	313.6	0.039	0.636	16
H → L+6 (20%), H → L+7 (64%)	4.108	301.8	0.051	0.710	14
H-5 → L (16%), H-3 → L+1 (72%)	4.273	290.1	0.022	0.453	10
H-1 → L+6 (40%), H-1 → L+7 (32%)	4.350	285.0	0.020	0.309	18
H-3 → L+2 (18%), H-1 → L+8 (70%)	4.450	278.7	0.030	0.418	16
CH_2Cl_2 solution					
H-1 → LUMO (10%), H → L (84%)	3.177	390.3	0.047	0.780	24
HOMO → L+1 (94%)	3.620	342.5	0.021	0.487	30
HOMO → L+2 (81%)	3.818	325.3	0.057	0.779	22
HOMO → L+5 (35%), HOMO → L+3 (31%)	3.900	317.9	0.069	0.848	7
HOMO → L+4 (55%)	4.012	309.1	0.176	1.339	10
H-1 → L+2 (83%)	4.082	303.7	0.022	0.466	27
H-1 → L+3 (33%), H-1 → L+4 (38%)	4.097	302.6	0.038	0.617	10
H-1 → L+3 (44%),	4.173	297.1	0.032	0.556	8
HOMO → L+7 (49%), HOMO → L+6 (26%)	4.241	292.3	0.075	0.881	10
H-3 → L+1 (42%), HOMO → L+10 (31%)	4.483	276.6	0.044	0.633	7
H-1 → L+6 (48%), H-1 → L+7 (34%)	4.517	274.5	0.028	0.493	13
H-2 → L+4 (50%), H-1 → L+7 (23%)	4.567	271.5	0.034	0.547	12
H-1 → L+8 (37%), H-2 → L+5 (23%)	4.606	269.2	0.020	0.425	8

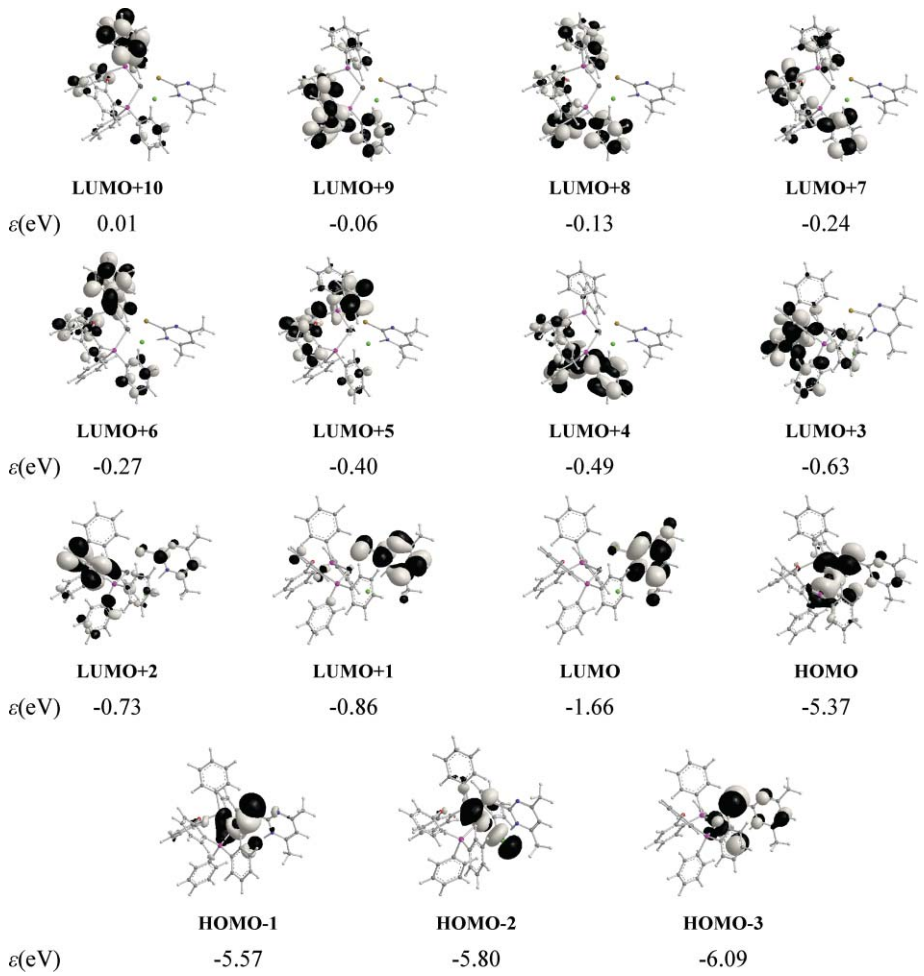

Fig. 5 Molecular orbitals involved in the electronic transitions of complex **7**.

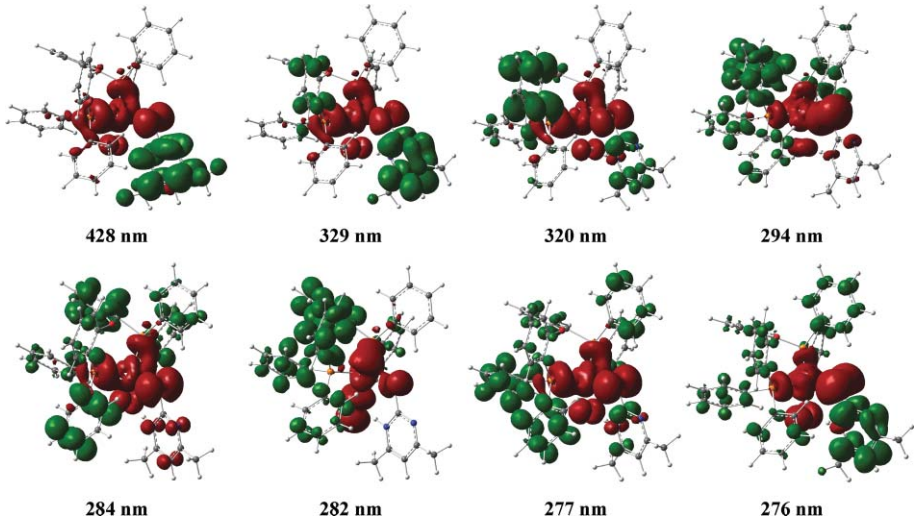

Fig. 6 Electron density difference maps corresponding to electronic transitions with high MLCT character in the absorption spectrum of complex **7**. Green and red colors show the regions of increased and decreased electron density, respectively.

mainly on the metal and the surrounding atoms, including S atom of thione and the halide ligands while HOMO-2 and HOMO-3 are constructed from out-of-phase combinations of Cu 3d AOs with p orbitals mainly located on the halide ligand and to a lesser extent on the S atom of the thione ligand. On the other hand, LUMO and LUMO+1 are located on the thione ligand while the rest of the unoccupied orbitals, involved in the electronic transitions of **1–9**, are mainly located in the phosphane ligands and thus the high-energy band could be assigned as MLL′CT/IL. It is worth noting that all the electronic transitions involved in the high-energy band are electric dipole allowed (non-zero transition dipole moment) and also that the corresponding %CT character of the electronic transitions, related to the high-energy band, is positive which is indicative of metal to ligand charge transfer. The latter is reflected on the EDDMs depicted in Fig. 6 *i.e.* clearly there is electron density depletion in the area comprising the metal and surrounding atoms and electron density enhancement in the areas including the phosphane and thione ligands.

Noteworthy, is the disappearance of the low-energy band as well as of the shoulder in the absorption spectra of the iodide complexes **3**, **6** and **9** in contrast to the chloride and bromide ones.

2.3.3 TD-DFT simulated emission spectra. The emission spectra of complexes **1–9**, were computed with TD-DFT calculations at the PEB0/Def2-TZVP level on the optimized first excited triplet state of the complexes both in the gas phase and in CH_2Cl_2 solution following a previously suggested methodology.[40,41] The simulated emission spectra for a representative complex **2** both in the gas phase and in CH_2Cl_2 solution are depicted schematically in Fig. 4, while those of the remaining complexes are given in ESI (Fig. S1 and S2).† Noteworthy, the simulated emission spectra perfectly resemble the experimental ones with respect to the region of 300–800 nm of the spectra. The simulated emission spectra of **1–9** exhibit the same qualitative pattern *i.e.* three or four sharp low-energy bands within the UV-Vis region (300–800 nm) which upon overlap afford one broad band perfectly matching the experimentally observed broad band (Fig. 2) and one or two broad high-energy bands within near-IR region (1000–1600 nm). Practically, changing the halide ligand merely alters the intensity of the bands. Thus, amongst complexes **1–6** with py2SH or pymtH thione ligands, the most intense bands are exhibited by those having chloride ligand while amongst complexes **7–9** with dmpymtH thione ligand, the iodide one exhibits the most intense bands. In addition, complexes with py2SH thione ligand show the most intense bands while the complexes with pymtH or dmpymtH thione ligands show bands of almost the same intensity. Finally, the emission spectra of complexes with pymtH ligand show four sharp low-energy bands in contrast to the emission spectra of the rest of the complexes which show three.

2.3.4 Vibrational analysis of the ground, S_0 and the lowest triplet, T_1 states. In order to help a future analysis of the vibronic structure of the phosphorescence spectra of complexes **1–9**, possibly with time resolved infrared spectroscopy, we calculated the vibrational frequencies and simulated the IR spectra for both their ground, S_0 and the lowest triplet, T_1 states. The simulated infrared spectra along with the normal modes of the most intense absorption bands for a representative complex **7** in both the ground, S_0 and the lowest triplet, T_1 states are depicted in Fig. 7.

The simulated IR spectra and normal modes of the rest of the complexes **2–9** both in their ground, S_0 and the lowest triplet, T_1 states exhibit quite similar features (Fig. S3–S10, ESI†). The bands at 519, 536, 730, 789 and 1511 cm^{-1} correspond to the out-of-plane bending of the atoms of the phenyl rings while the band at 3203 cm^{-1} corresponds to a 'breathing' mode of one phenyl ring. The bands at 1289, 1620 and 1679 cm^{-1} are related with in-plane deformations of the thione ligand. Finally, the band at 3115 cm^{-1} corresponds to N–H stretching vibration. Generally, the simulated IR spectra of complexes **1–9** are in close resemblance with the experimental ones. For example compare the scaled harmonic vibrational frequencies (scaling factor = 0.961)[42] of complex **7** with the experimental values given in parentheses:

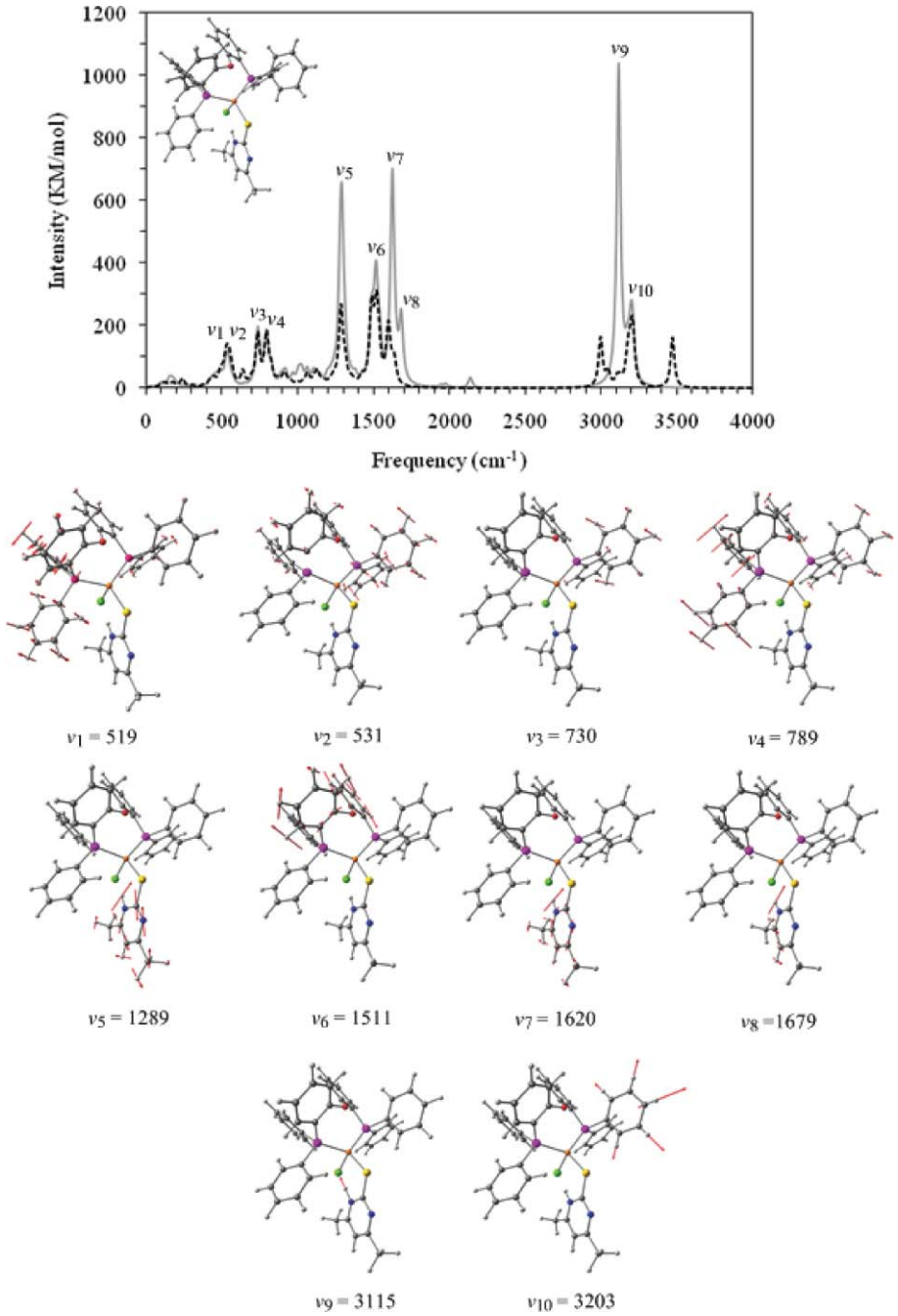

Fig. 7 Infrared spectra along with the normal modes of the most intense absorption bands of complex **7** in both the S_0 and T_1 states computed at the PEB0/Def2-TZVP level of theory (S_0 grey line, T_1 black/dashed line).

ν_9 = 3078.1, 2993.5 (3049 m), ν_8 = 1613.5 (1614 s), ν_7 = 1556.8 (1567vs), ν_6 = 1452.1 (1460 s), ν_5 = 1238.7 (1229 vs), ν_4 = 758.2 (748 s), ν_3 = 701.5 (737 s), ν_2 = 510.3 (511 s). Notice that the vibrational modes of the unmixed ground, S_0 and first triplet excited state, T_1 have almost identical frequencies. The only remarkable difference is a shift of the N–H stretching vibration to higher frequencies with a concomitant dramatic intensity decrease. This is indicative that upon $T_1 \rightarrow S_0$ de-excitation a hydrogen bond is formed between the H atom of the thione ligand and the halide ligand.

3. Experimental section

3.1 Materials and instrumentation

Commercially available copper(I) halides and bis[2-(diphenylphosphano)phenyl]ether were used as received while the thiones (Aldrich) were re-crystallized from hot ethanol prior to their use. All the solvents were purified by respective suitable methods and allowed to stand over molecular sieves. Infra-red spectra in the region of 4000–250 cm^{-1} were obtained

Table 5 Crystal data and structure refinements for [CuCl(DPEphos)-(dmpymtH)], **7**

	7
Molecular formula	$C_{42}H_{36}ClCuN_2OP_2S{\cdot}0.125C_2H_5OH$
Formula weight	783.48
T/K	120(2)
Wavelength/Å	0.71073
Crystal system	Monoclinic
Space group	$P2_1/c$
a/Å	15.3542 (2)
b/Å	16.8655 (4)
c/Å	14.7534 (3)
α/°	90
β/°	100.3890 (10)
γ/°	90
Volume/Å^3	3757.85 (13)
Z	4
Density (calculated)/Mg m^{-3}	1.385
Absorpt. coefficient/mm^{-1}	0.830
F(000)	1621
Crystal size/mm	0.18 × 0.11 × 0.08
Theta range for data collection	2.96 to 27.48°
Index ranges	$-19 <= h <= 19$ $-21 <= k <= 21$ $-19 <= l <= 19$
Reflections collected	39 667
Independent reflections	8557 [R(int) = 0.0573]
Completeness	99.4% (theta = 27.48°)
Data/restraints/parameters	8557/0/453
Max. and min. transmission	0.9366 and 0.8650
Refinement method	Full-matrix least-squares on F^2
Goodness-of-fit on F^2	1.059
Final R indices [$I > 2\sigma(I)$]	R_1 = 0.0497, wR_2 = 0.01008
R indices (all data)	R_1 = 0.0613, wR_2 = 0.1070
Final weighting scheme	Calc $w = 1/[\sigma^2(F_o^2) + (0.0228P)^2 + 9.1795P]$ where $P = (F_o^2 + 2F_c^2)/3$
Largest diff. peak and hole	0.556 and −0.462 e/Å^3

in KBr discs with a Perkin-Elmer 1430 spectrophotometer, while a Perkin-Elmer-Hitachi 200 spectrophotometer and a Hitachi F-7000 Fluorescence Spectrophotometer were used to obtain the electronic absorption and emission spectra respectively.

Melting points were measured in open tubes with a STUART scientific instrument and are uncorrected. Molar conductivities, magnetic susceptibility measurements and elemental analyses for carbon, nitrogen and hydrogen were performed as described previously.[27]

3.2 Crystal structure determination†

Single crystals suitable for crystal structure analysis were obtained by slow evaporation of an acetonitrile–ethanol solution of the complex at room temperature. X-Ray diffraction data were collected on an Enraf-Nonius Kappa CCD area-detector diffractometer. The programs DENZO[43] and COLLECT[44] were used in data collection and cell refinement. Details of crystal and structure refinement are compiled in Table 5. The structures were solved using program SIR97[45] and refined with program SHELX-97.[46] The SQUEEZE option of PLATON is used in order to remove the disorder of 1/8 of an ethanol molecule from the calculations. Molecular plots were obtained with program ORTEP-3.[47]

3.3 General procedure for the synthesis of complexes 1–9

To a suspension of 0.5 mmol of copper(I) halide (49.5 mg for CuCl, 71.7 mg for CuBr, 95.2 mg for CuI) in 30 cm^3 of dry dichloromethane, 269.3 mg (0.5 mmol) of bis[2-(diphenylphosphano)phenyl]ether was added and the mixture was stirred for two hours at 50 °C. The resulting clear solution was filtered of and then treated with the appropriate thione (0.5 mmol) dissolved in a small amount (~20 cm^3) of ethanol and the new reaction mixture was stirred for additional two hours at 50 °C. Slow evaporation of the clear solution at ambient afforded a microcrystalline solid, which was filtered off and dried *in vacuo*.

3.3.1 [CuCl(DPEphos)(py2SH)] (1). Yellow crystals (314 mg, 84%), m.p. 172 °C; Anal. Calcd for $C_{41}H_{33}NClCuOP_2S$: C, 65.77; H, 4.44, N: 1.87%; Found: C, 65.41; H, 4.41; N, 1.69%. IR (cm^{-1}): 3427 br, 3050 m, 1563 s, 1585 s, 1476 vs, 1459 vs, 1432 vs, 1258 s, 1222 vs, 1180 s, 1132 s, 1092 s, 1068 s, 991 m, 872 s, 800 m, 747 vs, 695 vs, 502 s. UV-Vis [λmax (nm), logε], (CH_2Cl_2): 275 (4.69), 390 (2.59).

3.3.2 [CuBr(DPEphos)(py2SH)] (2). Yellow crystals (396 mg, 91%), m.p. 197 °C; Anal. Calcd for $C_{41}H_{33}NBrCuOP_2S$: C, 62.08; H, 4.19; N, 1.77%; Found: C, 61.87; H, 4.24; N, 1.70%. IR (cm^{-1}): 3436 br, 3045 m, 1573 vs, 1585 s, 1471 s, 1460 s, 1433 vs, 1258 s, 1205 vs, 1180 s, 1133 vs, 1096 s, 1068 m, 985 s, 872 m, 808 m, 747 vs, 695 vs, 508 s. UV-Vis [λmax (nm), logε], (CH_2Cl_2): 289 (4.32), 387 (3.85).

3.3.3 [CuI(DPEphos)(py2SH)] (3). Yellow crystals (419 mg, 90%), m.p. 259 °C; Anal. Calcd for $C_{41}H_{33}NCuIOP_2S$: C, 58.61; H, 3.96; N, 1.67%; Found: C, 58.75; H, 4.04; N, 1.64%. IR (cm^{-1}): 3465 br, 3044 m, 1565 vs, 1472 s, 1457 vs, 1361 s, 1256 s, 1203 vs, 1180 m, 1130 vs, 1091 s, 1068 m, 992 m, 870 m, 801 m, 745 vs, 689 vs, 507 vs. UV-Vis [λmax (nm), logε], (CH_2Cl_2): 285 (4.09), 386 (3.58).

3.3.4 [CuCl(DPEphos)(pymtH)] (4). Yellow crystals (374 mg, 82%), m.p. 232 °C; Anal. Calcd for $C_{40}H_{32}N_2ClCuOP_2S$: C, 64.08; H, 4.30; N, 3.74%; Found: C, 63.80; H, 4.28; N, 3.67%. IR (cm^{-1}): 3435 br, 3046 m, 1603 s, 1575 vs, 1480 s, 1457 s, 1432 vs, 1457 s, 1432 vs, 1324 s, 1218 vs, 1182 vs, 1093 m, 976 s, 875 m, 745 s, 694 vs, 508 s, 466 s. UV-Vis [λmax (nm), logε], (CH_2Cl_2): 287 (4.35), 398 (3.24).

3.3.5 [CuBr(DPEphos)(pymtH)] (5). Yellow crystals (396 mg, 91%), m.p. 154 °C; Anal. Calcd for $C_{40}H_{32}N_2BrCuOP_2S$: C, 60.49; H, 4.06; N, 3.53%; Found: C, 60.36; H, 3.92; N, 3.54%. IR (cm^{-1}): 3452 br, 3048 m, 1612 vs, 1562 vs, 1459 s, 1433 vs, 1226 vs, 1210 vs, 1157 s, 1093 s, 983 m, 869 m, 747 vs, 738 vs, 696 vs, 511 s, 498 s. UV-Vis [λmax (nm), logε], (CH_2Cl_2): 286 (4.45), 385 (3.44).

3.3.6 [CuI(DPEphos)(pymtH)] (6). Orange crystals (418 mg, 85%), m.p. 208 °C; Anal. Calcd for $C_{40}H_{32}N_2ICuOP_2S$: C, 57.11; H, 3.83; N, 3.33%; Found: C, 56.96; H, 3.77; N, 3.34%. IR (cm^{-1}): 3435 br, 3050 m, 1606 s, 1565 s, 1461 s, 1492 vs, 1328 s, 1258 s, 1220 vs, 1189 s, 1093 m, 982 m, 872 m, 748 vs, 694 vs, 508 s, 473 s. UV-Vis [λmax (nm), logε], (CH_2Cl_2): 291 (4.46), 390 (3.38).

3.3.7 [CuCl(DPEphos)(dmpymtH)] (7). Yellow crystals (388 mg, 82%), m.p. 206 °C; Anal. Calcd for $C_{42}H_{36}ClCuN_2OP_2S$: C, 64.86; H, 4.66; N, 3.60%; Found: C, 63.53; H, 4.58; N, 3.45%.

IR (cm^{-1}): 3452 br, 3049 m, 1614 s, 1567 vs, 1460 s, 1432 vs, 1229 vs, 1206 vs, 1093 m, 986 m, 748 s, 737 s, 696 s, 511 s, 463 s. UV-Vis [λmax (nm), logε], (CH_2Cl_2): 278 (4.09), 393 (3.30).

3.3.8 [CuBr(DPEphos)(dmpymtH)] (8). Yellow crystals (410 mg, 85%), m.p. 197 °C; Anal. Calcd for $C_{42}H_{36}N_2BrCuOP_2S$: C, 61.35; H, 4.41; N, 3.41%; Found: C, 61.26; H, 4.50; N, 3.35%. IR (cm^{-1}): 3436 br, 3052 m, 1608 s, 1564 s, 1547 vs, 1462 s, 1434 vs, 1251 s, 1220 s, 1119 s, 1068 m, 741 s, 694 s, 507 s, 460 s. Vis [λmax (nm), logε], (CH_2Cl_2): 284 (4.02), 388 (3.31).

3.3.9 [CuI(DPEphos)(dmpymtH)] (9). Yellow crystals (434 mg, 82%), m.p. 146 °C; Anal. Calcd for $C_{42}H_{36}N_2ICuOP_2S$: C, 58.03; H, 4.17; N: 3.22%; Found: C, 58.06; H, 4.21; N, 3.24; IR (cm^{-1}): 3434 br, 3035 m, 1622 vs, 1562 vs, 1462 s, 1437 vs, 1219 vs, 1186 vs, 1029 m, 978 s, 746 s, 690 s, 537 m, 505 s, 459 s. Vis [λmax (nm), logε], (CH_2Cl_2): 290 (4.40), 380 (3.51).

3.4. Computational details

Full geometry optimization without symmetry constrains were carried out in the gas phase for both the singlet ground state (S_0) and the lowest triplet excited state (T_1) of complexes **1–9**, using the full-range PBE0 non-local hybrid GGA functional[48–51] combined with the Def2-TZVP basis set of Ahlrichs *et al.*[52] for all atoms (the computational protocol is denoted as PBE0/Def2-TZVP). The attainment of the energy minimum was verified by calculating the vibrational frequencies that result in the absence of imaginary eigenvalues (NImag = 0). The computed electronic energies were corrected to constant pressure and 298 K, for zero point energy (ZPE) differences and for the contributions of the translational, rotational and vibrational partition functions. Time-dependent density functional theory (TDDFT)[53–56] calculations were performed employing the PBE0/Def2-TZVP computational protocol. The TDDFT calculations were performed in the gas phase and in CH_2Cl_2 solution for both the singlet ground state (S_0) and the lowest triplet excited state (T_1) of complexes **1–9** including the lowest 50 singlet–singlet and triplet–triplet excitations. All calculations were done using the Gaussian03 program suite.[56] The Mulliken atomic spin densities were obtained by employing Mulliken population analysis.[57,58]

4. Concluding remarks

In this paper we have described the synthesis of nine novel mixed-ligand Cu(I) complexes **1–9**, bearing a bidentate phosphane and heterocyclic thiones as ligands. The new complexes are easily formed by the addition of the thione ligand to a CuX–diphosphane adduct in dichloromethane–ethanol solution. The X-ray structural analysis revealed that complex **7** adopts a slightly distorted tetrahedral geometry with the copper(I) metal centre surrounded by the P atoms of the bidentate DPEphos ligand, the chloride ligand and the S-donor atom of the dmpymtH ligand. The S-coordination mode of the latter could be verified by the appearance of the four characteristic 'thioamide bands' in the recorded IR spectra of the complexes **1–9**. The distorted tetrahedral structure as well as the S-coordination mode of the thione ligand to the Cu(I) metal center are further corroborated from DFT geometry optimizations of the structural parameters of complexes **1–9**. The electronic absorption spectra of these complexes show two broad bands in the regions 275–290 and 380–398 nm. According to TD-DFT calculations these bands could be assigned as having MLL′CT/IL character. An intense blue–green emission in the range 500–558 nm is observed for complexes of py2SH or dmpymtH thione ligands, while complexes of the pymtH ligand show only weak emission. However, based upon the TD-DFT simulated emission spectra both in the gas phase and in CH_2Cl_2 solution, it is expected to have additional emission bands in the UV-Vis and near-IR regions. The largest $\Delta E_{T_1-S_0}$ energy gap amongst all complexes under investigation is found for the complexes with pymtH ligand and therefore it is expected that they would have the largest nonradiative decay rate constant, k_{nr}. On the other hand, the computed Δdd_{occ} energy splitting values of complexes **1–9** present small variation making this parameter unsuitable for predicting the magnitude of radiative decay rate constants, k_r and phosphorescence efficiencies. The structural distortions associated with the T_1 to S_0 transitions are found to be relatively small and are also reflected on the computed IR spectra for these states. The only remarkable structural distortion upon $T_1 \rightarrow S_0$ de-excitation is a change in the thione conformational orientation resulting in N–H···X hydrogen bond formation. Concomitantly there is a shift to lower frequencies of the N–H stretching vibration mode, accompanied by a dramatic intensity increase.

Acknowledgements

We thank the EPSRC X-ray crystallography service at the University of Southampton for collecting the X-ray data. The authors aknowledge computer time provided by the Center for Scientific Simulations at the University of Ioannina, Greece.

References

1 J. C. Vickery, M. M. Olmstead, E. Y. Fung and A. L. Balch, *Angew. Chem., Int. Ed. Engl.*, 1997, **36**, 1179.
2 M. A. Mansour, W. B. Connick, R. J. Lachicotte, H. J. Gysling and R. Eisenberg, *J. Am. Chem. Soc.*, 1998, **120**, 1329.
3 J. N. Demas and B. A. de Graff, *Coord. Chem. Rev.*, 2001, **211**, 317.
4 K. E. Erkkila, D. T. Odom and J. K. Barton, *Chem. Rev.*, 1999, **99**, 2777.
5 C. H. Chen and J. Shi, *Coord. Chem. Rev.*, 1998, **171**, 161.
6 C. M. Elliott, F. Pichot, C. J. Bloom and L. S. Rider, *J. Am. Chem. Soc.*, 1998, **120**, 6781.
7 B. Minaev, E. Jansson and H Ågren, *J. Chem. Phys.*, 2006, **125**, 234704.
8 B. Minaev, E. Jansson, S. Scrader and H Ågren, *Chem. Phys.*, 2007, **333**, 157.
9 H. Yersin, *Top. Curr. Chem.*, 2004, **241**, 1.
10 C. A. Bignozzi, R. Argazzi and C. J. Kleverlaan, *Chem. Soc. Rev.*, 2000, **29**, 87.
11 D. Felder, J. F. Nierengarten, F. Barigelletti, B. Ventura and N. Armaroli, *J. Am. Chem. Soc.*, 2001, **123**, 6291.
12 D. V. Scaltrito, D. W. Thompson, J. A. O'Callaghan and G. J. Meyer, *Coord. Chem. Rev.*, 2000, **208**, 243.
13 M. Cantuel Lavie-Cambot, Y. Leydet, G. Jonusauskas, D. M. Bassani and N. D. McClenaghan, *Coord. Chem. Rev.*, 2008, **252**, 2572.
14 N. Armaroli, *Chem. Soc. Rev.*, 2001, **30**, 113, and references therein.
15 D. R. McMillin and K. M. McNett, *Chem. Rev.*, 1998, **98**, 1201.
16 D. G. Guttell, S.-M. Kuang, P. E. Fanwick, D. R. McMillin and R. A. Walton, *J. Am. Chem. Soc.*, 2002, **124**, 6.
17 N. Armaroli, G. Accorsi, M. Holler, O. Moudam, J.-F. Nierengarden, Z. Zhou, R. T. Wegh and R. Welter, *Adv. Mater.*, 2006, **18**, 1313.
18 L. Yang, J. K. Feng, A. M. Ren, M. Zhang, Y. G. Ma and X. D. Liu, *Eur. J. Inorg. Chem.*, 2005, 1867.
19 S. M. Kuang, D. G. Guttell, D. R. McMillin, P. E. Fanwick and R. A. Walton, *Inorg. Chem.*, 2002, **41**, 3313.

20 Q. Zhang, J. Ding, Y. Cheng, L. Wang, Z. Xie, X. Jing and F. Wang, *Adv. Funct. Mater.*, 2007, **17**, 2983.
21 M. W. Blaskie and D. R. McMillin, *Inorg. Chem.*, 1980, **19**, 3519.
22 C. T. Cunningham, J. J. Moore, K. L. H. Cunningham, P. E. Fanwick and D. R. McMillin, *Inorg. Chem.*, 2000, **39**, 3638.
23 D. Felder, J.-F. Nierengarten, F. Barigelletti, B. Ventura and N. Armaroli, *J. Am. Chem. Soc.*, 2001, **123**, 6291.
24 K. Shinozaki and Y. Kaizu, *Bull. Chem. Soc. Jpn.*, 1994, **67**, 2435.
25 L. Yang, J-K. Feng, A.-M. Ren, M. Zhang, Y.-G. Ma and X.-D. Liu, *Eur. J. Inorg. Chem.*, 2005, 1867.
26 Z. A. Siddique, Y. Yamamoto, T. Ohno and K. Nozaki, *Inorg. Chem.*, 2003, **42**, 6366.
27 P. Aslanidis, P. J. Cox, K. Kapetangiannis and A. C. Tsipis, *Eur. J. Inorg. Chem.*, 2008, 5029.
28 Z.-N. Chen, N. Zhao, Y. Fan and J. Ni, *Coord. Chem. Rev.*, 2009, **253**, 1.
29 S.-M. Kuang, D. G. Cuttell, D. R. McMillin, P. E. Fanwick and R. A. Walton, *Inorg. Chem.*, 2002, **41**, 3313.
30 D. G. Cuttell, S.-M. Kuang, P. E. Fenwick, D. R. McMillin and R. A. Walton, *J. Am. Chem. Soc.*, 2002, **124**, 6.
31 Yi.-M. Xie and J.-H. Wu, *Inorg. Chem. Commun.*, 2007, **10**, 1561.
32 R. Venkateswaran, M. S. Balakrishna, S. M. Mobin and H. M. Tuononen, *Inorg. Chem.*, 2007, **46**, 6535.
33 P. J. Cox, P. Aslanidis, P. Karagiannidis and S. K. Hadjikakou, *Polyhedron*, 1999, **18**, 1501.
34 P. Aslanidis, S. K. Hadjikakou, P. Karagiannidis and P. J. Cox, *Inorg. Chim. Acta*, 1998, **271**, 243.
35 G. P. Voutsas, S. C. Kokkou, C. J. Cheer, P. Aslanidis and P. Karagiannidis, *Polyhedron*, 1995, **14**, 2287.
36 S. Skoulika, A. Aubry, P. Karagiannidis, P. Aslanidis and S. Papastefanou, *Inorg. Chim. Acta*, 1991, **183**, 207.
37 J. R. Lakowicz, *Principles of fluorescence spectroscopy*, 3rd ed., 2006, XXVI, 954 Springer-Verlag.
38 F. Rausch, H. H. H. Homeier, P. I. Djurovich, M. E. Thompson and H. Yersin, *Proc. SPIE*, 2007, **6655**, 66550F.
39 H. Yersin, W. J. Finkenzeller in *Highly Efficient OLEDs with Phosphorescent Materials*, ed. H. Yersin, Wiley-VCH, Weinheim, 2008, 1.
40 D. Jacquemin, E. A. Perpète, G. Scalmani, M. J. Frisch, I. Ciofini and C. Adamo, *Chem. Phys. Lett.*, 2006, **421**, 272.
41 D. Jacquemin, E. A. Perpète, X. Assfeld, G. Scalmani, M. J. Frisch and C. Adamo, *Chem. Phys. Lett.*, 2007, **438**, 208.
42 Y. Tantirungrotechai, K. Phanasant, S. Roddecha, P. Surawatanawong, V. Sutthikhum and J. Limtrakul, *THEOCHEM*, 2006, **760**, 189.
43 Z. Otwinowski, W. Minor, in *Macromolecular Crystallography*, ed. C. W. Carter Jr. and R. M. Sweet, Academic Press, New York, Part A, vol. 276.
44 R. Hooft, COLLECT *Data Collection Software*. Nonius BV, 1998.
45 M. C. Burla Altomare, M. Camalli, G. L. Cascarano, C. Giacovazzo, A. Guagliardi, A. G. G. Moliterni, G. Polidori and R. Spagna, *J. Appl. Crystallogr.*, 1999, **32**, 115.
46 G. M. Sheldrick, SHELXL-97. *Program for Crystal Strucutre Analysis* (Release 97-2), University of Göttingen, Germany, 1997.
47 L. J. Farrugia, *J. Appl. Crystallogr.*, 1997, **30**, 565.
48 J. P. Perdew, K. Burke and M. Ernzerhof, *Phys. Rev. Lett.*, 1996, **77**, 3865.
49 C. Adamo and V. Barone, *Chem. Phys. Lett.*, 1997, **274**, 242.
50 C. Adamo and V. Barone, *J. Chem. Phys.*, 1999, **110**, 6158.
51 M. Ernzerhof and G. E. Scuseria, *J. Chem. Phys.*, 1999, **110**, 5029.
52 F. Weigend and R. Ahlrichs, *Phys. Chem. Chem. Phys.*, 2005, **7**, 3297.
53 S. J. A. van Gisbergen, F. Kootstra, P. R. T. Schipper,O. V. Gritsenko, J. G. Snijders and E. J. Baerends, *Phys. Rev. A: At., Mol., Opt. Phys.*, 1998, **57**, 2556.
54 R. Bauernschmitt and R. Ahlrichs, *Chem. Phys. Lett.*, 1996, **256**, 454.
55 C. Jamorski, M. E. Casida and D. R. Salahub, *J. Chem. Phys.*, 1996, **104**, 5134.
56 *Gaussian 03*, Revision E.01, M. J. Frisch, G. W. Trucks, H. B. Schlegel, G. E. Scuseria, M. A. Robb, J. R. Cheeseman, J. A. Montgomery, Jr., T. Vreven, K. N. Kudin, J. C. Burant, J. M. Millam, S. S. Iyengar, J. Tomasi, V. Barone, B. Mennucci, M. Cossi, G. Scalmani, N. Rega, G. A. Petersson, H. Nakatsuji, M. Hada, M. Ehara, K. Toyota, R. Fukuda, J. Hasegawa, M. Ishida, T. Nakajima, Y. Honda, O. Kitao, H. Nakai, M. Klene, X. Li, J. E. Knox, H. P. Hratchian, J. B. Cross, V. Bakken, C. Adamo, J. Jaramillo, R. Gomperts, R. E. Stratmann, O. Yazyev, A. J. Austin, R. Cammi, C. Pomelli, J. W. Ochterski, P. Y. Ayala, K. Morokuma, G. A. Voth, P. Salvador, J. J. Dannenberg, V. G. Zakrzewski, S. Dapprich, A. D. Daniels, M. C. Strain, O. Farkas, D. K. Malick, A. D. Rabuck, K. Raghavachari, J. B. Foresman, J. V. Ortiz, Q. Cui, A. G. Baboul, S. Clifford, J. Cioslowski, B. B. Stefanov, G. Liu, A. Liashenko, P. Piskorz, I. Komaromi, R. L. Martin, D. J. Fox, T. Keith, M. A. Al-Laham, C. Y. Peng, A. Nanayakkara, M. Challacombe, P. M. W. Gill, B. Johnson, W. Chen, M. W. Wong, C. Gonzalez and J. A. Pople, Gaussian, Inc., Wallingford CT, 2004.
57 R. S. Mulliken, *Phys. Rev.*, 1932, **41**, 66.
58 R. S. Mulliken, *J. Chem. Phys.*, 1935, **3**, 573; R. S. Mulliken, *J. Chem. Phys.*, 1995, **23**, 1833, 2343, 2388.